ACS APPLIED MATERIALS & INTERFACES

www.acsami.org

Research Article

Enhanced Thermal Conductivity in Oriented Polyvinyl Alcohol/Graphene Oxide Composites

Xinglong Pan, Michael G. Debije, Albert P. H. J. Schenning,* and Cees W. M. Bastiaansen*

Cite This: *ACS Appl. Mater. Interfaces* 2021, 13, 28864–28869

Read Online

ACCESS | Metrics & More | Article Recommendations | Supporting Information

ABSTRACT: Polymer composites have attracted increasing interest as thermal management materials for use in devices owing to their ease of processing and potential lower costs. However, most polymer composites have only modest thermal conductivities, even at high concentrations of additives, resulting in high costs and reduced mechanical properties, which limit their applications. To achieve high thermally conductive polymer materials with a low concentration of additives, anisotropic, solid-state drawn composite films were prepared using water-soluble polyvinyl alcohol (PVA) and dispersible graphene oxide (GO). A co-additive (sodium dodecyl benzenesulfonate) was used to improve both the dispersion of GO and consequently the thermal conductivity. The hydrogen bonding between GO and PVA and the simultaneous alignment of GO and PVA in drawn composite films contribute to an improved thermal conductivity (~25 W m^{-1} K^{-1}), which is higher than most reported polymer composites and an approximately 50-fold enhancement over isotropic PVA (0.3−0.5 W m^{-1} K^{-1}). This work provides a new method for preparing water-processable, drawn polymer composite films with high thermal conductivity, which may be useful for thermal management applications.

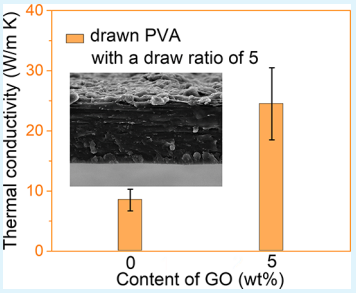

KEYWORDS: *thermal conductivity, polyvinyl alcohol, graphene oxide, orientation, hydrogen bonding*

INTRODUCTION

Due to their ease of processing, high corrosion and electrical resistances, and relatively low costs and weight, polymers are widely used in daily life.[1−3] However, bulk polymers generally have relatively low thermal conductivities (usually <1 W m^{-1} K^{-1}), which limit their application as thermal management materials for heat exchangers, electronic devices, and solar cells, for example.[3−7]

The thermal conductivity of polymers can be enhanced by adding fillers with high thermal conductivity.[3−10] Typically, thermally conductive nanocarbon materials including graphite nanoplatelets, carbon nanotubes, graphene, and their derivatives are blended as additives into the polymer matrix to achieve an increased thermal conductivity.[4,6,8] Still, the thermal conductivity of isotropic polymer composites with a high concentration of additives is <10 W m^{-1} K^{-1} due to the poor compatibility and interaction between the polymer matrix and additives, resulting in poor dispersion of the additives and serious phonon scattering[3−6] as well as the deterioration of the mechanical properties of the composites.

Recently, high thermal conductivities in anisotropic polymers, including polyethylene (PE) microfilms and micro/nanofibers,[10−14] polyvinyl alcohol (PVA) microfilms,[15−17] polyamide nanofibers,[18] and their composite films, have been demonstrated via high degrees of chain orientation, chain extension, and crystallinity. For instance, stretched polyethylene containing graphene nanoplatelets (draw ratio of ~5) showed a thermal conductivity of ~6 W m^{-1} K^{-1} with a weak van der Waals interaction at the interfaces between the polyethylene and graphene nanoplatelets.[7] Combined high thermal conductivity (~75 W m^{-1} K^{-1}) and visible transparency were obtained using polyethylene with 0.1 wt % graphene and a low melting point compatibilizer (2-(2*H*-benzotriazol-2-yl)-4,6-ditertpentylphenol, BZT) at a draw ratio of 100.[9]

As previously reported, enhanced intermolecular interactions between the polymer chains and the additives are an advantage for obtaining high thermal conductivity in drawn composite films.[9,19−21] While anisotropic polymer composites with high thermal conductivities have been reported for stretched polyethylene, to date studies of more polar anisotropic polymer composites, like PVA films employing green processes (that is, avoiding organic solvents), have been less prevalent. PVA is an atactic, water-soluble polymer with an orthorhombic unit cell and planar zigzag configuration similar to polyethylene, resulting in dense packing in the crystal lattice with a high theoretical modulus, strength, and thermal conductivity.[16,22,23]

Received: April 7, 2021
Accepted: June 1, 2021
Published: June 8, 2021

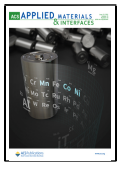

Here, we report high thermal conductivities in anisotropic PVA/graphene oxide (GO) composite films containing a second additive (SDBS) produced via casting and solid-state drawing. We demonstrate that the combination of hydrogen bonding between GO and aligned PVA contributes to an improved thermal conductivity (~25 W m^{-1} K^{-1}) in PVA/GO composite films, greater than that of most polymer composites.

EXPERIMENTAL SECTION

Materials. PVA flakes (M_w = 146,000−186,000 Da, 99+% hydrolyzed, CAS number: 9002-89-5, product number: 363065), GO nanoplatelets (brown/black powder, layers: 15−20, edge oxidization: 4−10%, product number: 796034), and sodium dodecyl benzenesulfonate (SDBS, CAS number: 25155-30-0, product number: 289957) were purchased from Sigma-Aldrich and used without further purification.

Fabrication. GO and SDBS were dispersed in deionized water (50 mL) using ultrasonication (Branson 1510 ultrasonic cleaner, 80 W) for 1 h. The composition of the films after casting and drying is shown in Table 1. PVA flakes (5 g) were added to the mixture with vigorous stirring at 98 °C and then dissolved with reflux for 4 h. The mixture was cast into polystyrene Petri dishes with an area of ~300 cm^2. After drying at 60 °C for 2 days, the composite films were drawn at 130 °C to a draw ratio of ~5.

Table 1. Contents of Elements in Drawn Composite Films

samples	PVA (g)	GO (mg)	SDBS (mg)
PVA-0	5	0	0
PVA-1	5	50	50
PVA-2	5	100	50
PVA-5	5	250	50
PVA-0(2)	5	0	50
PVA-5(2)	5	250	0
PVA-5(3)	5	250	250

Analytical Techniques. The thermal conductivity of drawn composite films along the drawing direction was measured based on the Angstrom method, as reported earlier.[9,10] 2D wide-angle X-ray scattering (WAXS) was performed on a Ganesha lab instrument equipped with a Genix-Cu ultralow divergence source producing 0.154 nm X-rays. Diffraction patterns were collected for 15 min on a Pilatus 300 K silicon pixel detector. The plane of measured films is perpendicular or parallel to the incident X-ray. Herman's orientation function of the composite films was calculated from the full width at half-maximum (FWHM) of the azimuthally scanned peak.[24,25] Polarized and non-polarized Fourier transform infrared (FTIR) spectra were measured on a Varian 670-IR spectrometer equipped with a golden gate setup with and without a polarizer. Raman scattering spectroscopy was performed on a Raman microscope (Witec Alpha 300 R) using a 532 nm laser. Photographs of composite films were taken using a Canon camera. Optical microscopy (OM) images of samples were performed on a Leica DM 2700 M microscope without polarizers. The temperatures of composite films were recorded using an infrared (IR) camera (Fluke). One end of the drawn films was affixed to one side of a copper plate with a high thermal conductivity with double-sided carbon tape (NEM tape, Nisshin EM. Co. Ltd), and the distal edge of the copper plate was placed on a hot plate set to 194 F (80 °C). The temperatures of the films at similar positions were recorded at 0 and 2 min after placement on the hot plate. For measurement of the cooling cycle, composite films were attached to the top of stainless-steel pillars with double-sided carbon tape. The pillars were fixed to the surface of an aluminum plate, which was heated on a hot plate to 194 F (80 °C) for 10 min until thermal equilibrium was attained. Then, the entire assembly was removed from the hot plate and left to cool to room temperature. Stainless steel was used rather than copper to retard the cooling process (due to the lower thermal conductivity of stainless steel compared to copper) so that the difference in temperature between the drawn films could be more easily measured. The cooling measurements were repeated several times to accurately record the temperature of the films drawn with and without additives. Scanning electron microscopy (SEM; JSM-IT100, JEOL, secondary electron detector) images of samples were recorded with a beam current of 10 kV (magnification from 700 to 3000×) after breaking the samples in liquid nitrogen and sputtering with platinum (Pt). Characterization of GO was accomplished by dispersing as powder in alcohol and then dropping on a silicon wafer. After drying, the dispersed GO on the wafer was sputtered for 30 s with Pt at a current of 30 mA. Measurement of electrical conductivity of drawn PVA-5 films was

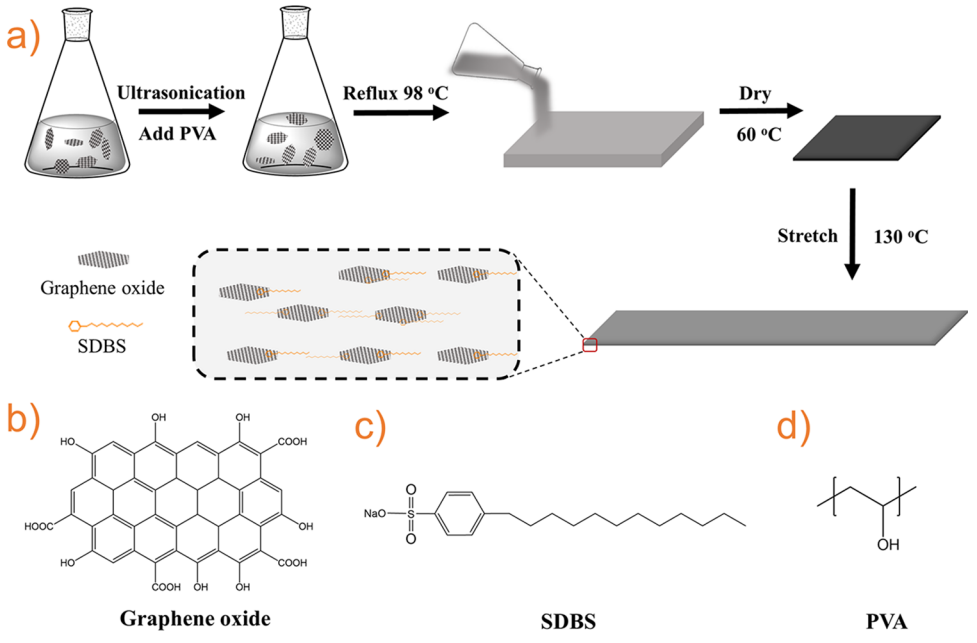

Figure 1. (a) Fabrication process for drawn PVA composite films. (b−d) Chemical structures of graphene oxide (GO, simplified chemical structure), sodium dodecyl benzenesulfonate (SDBS), and PVA.

https://doi.org/10.1021/acsami.1c06415
ACS Appl. Mater. Interfaces 2021, 13, 28864−28869

performed on a SourceMeter (KEITHLEY, 2400) with a voltage of 10 volts. The mechanical properties of PVA-5 films were performed using dynamic mechanical analysis (DMA) from 25 to 90 °C with a frequency of 1 Hz and a strain of 0.5%, while Young's modulus of drawn PVA composite films was measured at ~25.5 °C using DMA.

RESULTS AND DISCUSSION

To obtain homogeneous PVA/GO composite films, PVA, GO, and SDBS were employed (Figure 1). SDBS, which has a high melting point (~200 °C), was included as a compatibilizer, while GO was used instead of graphene to enhance the dispersion in PVA. The resulting solution/dispersion was poured into polystyrene molds and dried at 60 °C for 2 days. The composite films were then stretched at 130 °C to a draw ratio of ~5. The effects of GO (0−5 wt %) and SDBS (0−5 wt %) concentrations and draw ratios were systematically studied in the drawn polymer films (see Table 1: for this paper, the nomenclature PVA-*n* generally represents a drawn PVA composite film containing *n* wt % GO, variable amounts of SDBS, and is drawn to a ratio of 5). Higher concentrations of GO (>5 wt %) were not studied due to the generally poor dispersion and stretchability of the composite films.

The thermal conductivities of the drawn PVA/GO composite films were measured as a function of the concentration of GO (Figure 2a), revealing that the thermal conductivity increases with increasing concentration of GO. The highest thermal conductivity, ~25 W m^{-1} K^{-1}, was obtained with drawn PVA-5, exhibiting approximately 3 times the thermal conductivity of drawn neat PVA-0 films and an approximately 50-fold enhancement in thermal conductivity in comparison to pure, isotropic PVA-0 (Figure 2d and Table S1).

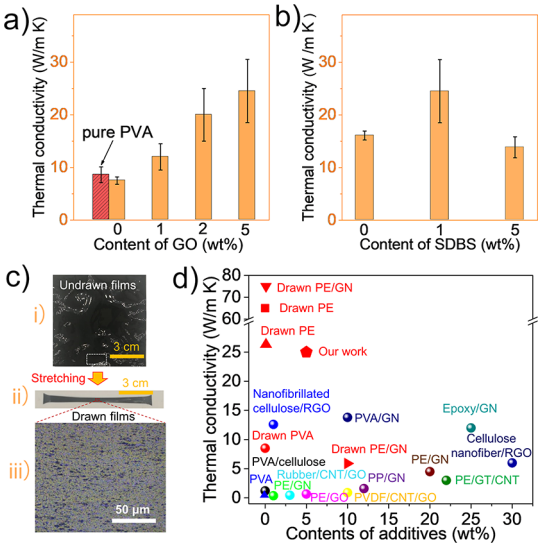

Figure 2. (a) Thermal conductivity of drawn pure PVA-0 without SDBS (red block) and thermal conductivities of PVA-0(2), PVA-1, PVA-2, and PVA-5 films, each containing 1 wt % SDBS with an increasing GO content. (b) Thermal conductivities of drawn PVA-5(2), PVA-5, and PVA-5(3) films containing variable concentrations of SDBS with 5 wt % of GO. (c) Photographs of undrawn (i) and drawn (ii) PVA-5 films and the OM image (iii) of drawn PVA-5 films. (d) Thermal conductivities reported for different films in the literature.[9,10,13,15,16,23−30] The *x* axis represents the wt % contents of the thermally conductive additives. The red symbols represent drawn polymers or composites. Here, GN, RGO, GT, CNT, and PVDF represent graphene, reduced graphene oxide, graphite, carbon nanotube, and polyvinylidene fluoride, respectively.

The role of the SDBS surfactant was also studied (Figure 2a,b). The thermal conductivity of drawn PVA-0(2) decreases with the addition of SDBS compared to PVA-0 (Figure 2a), which may be expected since the addition of low molecular weight additives commonly reduces thermal conductivity.[9] In contrast, adding SDBS (up to 1 wt %) increases the thermal conductivity of drawn PVA-5 (compared to PVA-5(2)): further increasing the SDBS content to 5 wt % (sample PVA-5(3)) results in the thermal conductivity decreasing again (Figure 2b). Apparently, adding up to 1 wt % of the surfactant likely enhances the dispersion of GO (Figure S1), but the poor thermal conductivity of SDBS dominates at higher contents, resulting in an overall lower conductivity. The experimental data in Figure 2 also show that adding GO without SDBS increases the thermal conductivity from ~8 to ~16 W m^{-1} K^{-1}, which illustrates that the increase in thermal conductivity (from ~8 to ~25 W m^{-1} K^{-1}; Figure 2a) originates partly from both additives. The mechanical effects of adding SDBS were examined using DMA (Figure S2 and Table S2). The results indicate that a high content of SDBS decreases the storage modulus and increases tan δ. In other words, SDBS behaves as a mechanical plasticizer, especially at high SDBS contents. Please note that a very high SDBS content was used here (5 wt %), which is far greater than the optimum SDBS content (1 wt %). In addition, Young's modulus decreases with the addition of SDBS, while the maximum draw ratio increases (Table S2), probably further resulting from the addition of SDBS as a plasticizer.

Photographs of undrawn and drawn PVA-5 films are shown in Figure 2c, i and ii. The OM image of the drawn PVA-5 film indicates that the addition of both additives (GO and SDBS) improves the dispersion (compare Figure S3 and Figure 2c, iii), although there is aggregation due to the excessive content of GO in PVA films. In Figure 2d, the thermal conductivity of a wide variety of undrawn and drawn films described in the literature is shown as a function of the content of thermally conductive additives, including graphene, carbon nanotubes, graphene oxide, and mixtures (Table S1),[9,10,13,15,16,23−33] revealing the impressive thermal conductivity in drawn PVA-5 films with low additive contents. Drawn PE and PE/GN films showed greater thermal conductivity than drawn PVA/GO films in this work, probably due to the high orientation and crystallinity induced by ultrahigh draw ratios in drawn PE and PE/GN films, which could not be obtained in PVA/GO films.[10,11]

WAXS was performed to further analyze the drawn PVA/GO films (Figure 3a,b and Figure S4a,d). Undrawn PVA-0 films without additives show two scattering rings of lattice planes of (101) at $2\Theta \approx 19.5°$ and (100) at $2\Theta \approx 11.6°$, corresponding to the PVA crystalline domains (Figure S4a), while these scattering rings coalesce into scattering dots in drawn PVA films (Figure 3a), indicating some alignment of PVA crystalline domains. A significant amorphous halo is also observed in both films, indicating little orientation, to be expected at these low draw ratios.

In the case of the polymer composite films, the scattering rings of PVA (at 11.6 and 19.5°) (Figure S4c) also transform into scattering dots upon stretching (Figure 3b), revealing the alignment of PVA and suggesting a low through-plane alignment of GO, although the scattering rings of GO (lattice plane: (002), 2Θ: ~25.5°) transform into weak scattering arcs

https://doi.org/10.1021/acsami.1c06415
ACS Appl. Mater. Interfaces 2021, 13, 28864−28869

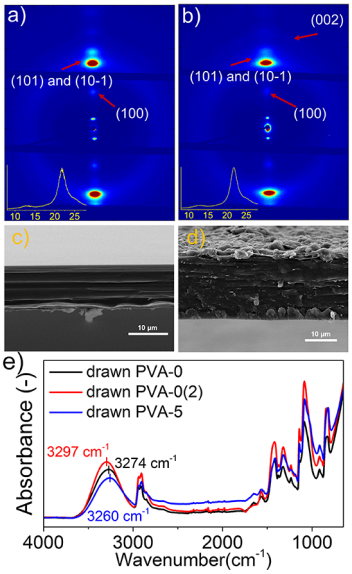

Figure 3. WAXS patterns of drawn PVA-0 (a) and drawn PVA-5 (b) composite films. The insets are the 1D curves of X-ray scattering. Here, the plane of measured films is perpendicular to the incident X-ray (Figure S5). SEM images of the cross section of drawn PVA-0 (c) and drawn PVA-5 (d) composite films. (e) Non-polarized FTIR spectra of drawn PVA-0, PVA-0(2), and PVA-5.

(Figure 3b). Herman's orientation function calculated by the full width at half-maximum (FWHM)[24,25] reveals that both the drawn PVA films with and without graphene (PVA-0 and PVA-5) have a high degree of orientation (~0.9) of the crystalline domains of PVA, indicating that there is no obvious effect of adding GO and SDBS. Anisotropy of SDBS in drawn PVA-5 films was also observed in the WAXS patterns due to the fact that the scattering rings of SBDS in undrawn films (Figure S5c) transfer into dots in drawn films (Figure S5d). Figure S5c reveals anisotropic GO in the plane of drawn PVA-5 films. These results suggest drawing-induced, simultaneous alignment of PVA and GO, similar to drawn PE and graphene films in the literature.[8,16] In the cross section of SEM (Figure 3c,d), the drawn PVA-0 and PVA-5 films show more aligned and fibrillar structures than undrawn PVA-0 and PVA-5 films (Figure S4e,g). Homogeneous dispersion of GO in PVA-5 films is observed in Figure S6a,b; the morphology of GO is characterized in Figure S6c,d, indicating that the size of GO is smaller than 2 μm, which is smaller than that in Figure 2, probably due to aggregation or the interlayer splitting induced by stretching.[16]

The interaction between PVA and the additives was investigated using infrared spectroscopy. FTIR spectra of drawn PVA-0 films with and without 1 wt % SDBS (Figure 3e and Figure S7a) show vibration peaks at ~3274 and 3297 cm^{-1}, respectively, attributed to the −OH group of PVA. In contrast, the drawn PVA films with 5 wt % GO and 1 wt % SDBS show a red-shifted (to lower energies/wavenumbers) peak at ~3260 cm^{-1}, indicating the hydrogen bonding interaction between GO and PVA (Figure S7a).[16,34,35] Although WAXS results indicate the orientation of the PVA chains, there is no obvious orientation of hydrogen bonding in the polarized FTIR spectra (Figure S7b,c), consistent with a previous literature report.[17] There is a drawing-induced shift to higher energies/wavenumbers of the absorption peak of −OH in both PVA-0 and PVA-5 films in comparison with the undrawn PVA-0 and PVA-5 films, respectively (Figure S7a), as reported as undrawn and drawn polyacrylonitrile and PVA in the literature.[36,37] FTIR spectra of pure SDBS powder and the undrawn PVA-0(2) film are shown in Figure S8 as control experiments, and the Raman spectrum confirms the oxidization group-induced defects in the GO powder (Figure S7d).

Simple setups were created to do a basic thermal analysis of representative composite films and to explore their potential application as heat transport and heat release elements (Figure 4). First, the ends of three films are fixed to the right end of a copper plate, and the left end of the copper plate was exposed to 194 F (80 °C) at time = 0 min (Figure 4b). After 2 min, the drawn PVA-5 film shows the highest temperature, while the undrawn PVA-5 film exhibits the lowest temperature at the same position (Figure 4c), indicating a higher thermal transport and thermal conductivity in the drawn PVA-5 film than both drawn PVA-0 and undrawn PVA-5 films. After heating, a cooling experiment was conducted to help clarify the heat release process of the composite films (Figure 4d,f). For the cooling measurement, the ends of two drawn films, one PVA-0 and the other PVA-5, were fixed atop stainless steel pillars, as shown in Figure 4d, and exposed to 194 F (80 °C) for 10 min, before removing the entire setup to ambient conditions, and the decrease in sample temperature was recorded (Figure 4e). The drawn PVA-5 film exhibited a greater temperature decrease and a lower final temperature after 2 min than the drawn PVA-0 film (Figure 4f), demonstrating that the drawn PVA-5 films more effectively

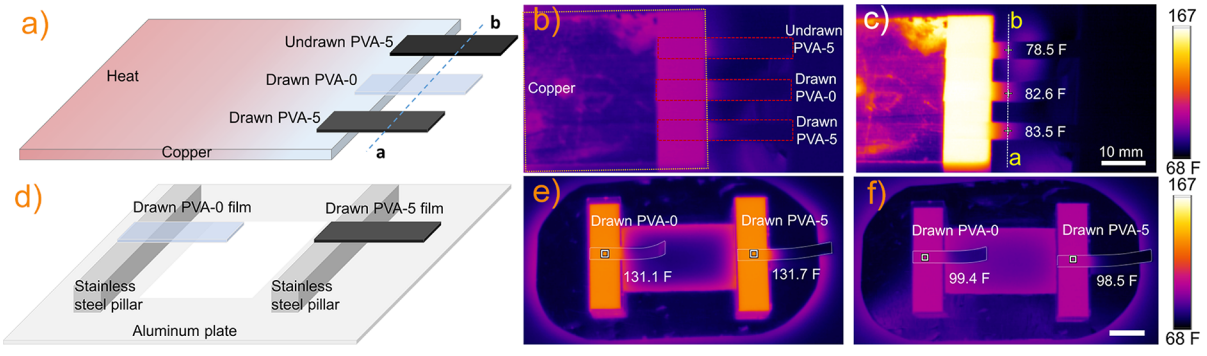

Figure 4. Schematic pictures of the thermal analysis module in the heating (a) and cooling (d) processes. (b, c) Thermal analysis of undrawn PVA-5, drawn PVA-0, and drawn PVA-5 films of similar sizes (highlighted by the dotted red boxes) during the heating process. (e, f) Thermal analysis of the drawn PVA-0 and PVA-5 films (highlighted by the dotted white boxes) during the cooling process. F is Fahrenheit.

https://doi.org/10.1021/acsami.1c06415
ACS Appl. Mater. Interfaces 2021, 13, 28864−28869

release heat, which makes them potentially useful in devices as thermal management materials.

CONCLUSIONS AND OUTLOOK

This work provides a new method for producing water-based polymer drawn films with high thermal conductivity, which are potentially useful for thermal management in electrical devices, like foldable video screens and flexible solar cells.

Oriented PVA/GO composite films were fabricated through water evaporation and solid-state stretching. SEM images and WAXS results reveal the improved dispersion of GO and the high orientation in drawn PVA/GO films when the co-additive (SDBS) is used. FTIR spectra of composite films demonstrated the presence of hydrogen bonding between PVA and GO. These results contributed to the high thermal conductivity of drawn PVA-5 composite films in the drawing direction, which is higher than most composite films and approximately a 50-fold enhancement in comparison with isotropic PVA.

It is tempting to speculate further on the applications of these films in, for instance, flexible solar cells and foldable video screens. For instance, solar cells usually have an efficiency below 25% and the residual absorbed energy is transferred into heat. The heating-up of the devices can be quite significant (100 °C), which actually reduces their efficiency and lifetime enormously. To satisfy the need in the foldable and flexible devices, the light density and flexible thermally conductive polymer composites were presented in this work.

ASSOCIATED CONTENT

Supporting Information

The Supporting Information is available free of charge at https://pubs.acs.org/doi/10.1021/acsami.1c06415.

High-resolution images of GO and cross-sectional images of PVA-5 films, DMA data of drawn PVA composite films, FTIR spectra of PVA films, Raman spectrum of GO, WAXS and FTIR spectrum of SDBS, and thermal conductivities of composite films in the literature (PDF)

AUTHOR INFORMATION

Corresponding Authors

Albert P. H. J. Schenning − *Laboratory of Stimuli-responsive Functional Materials & Devices (SFD), Department of Chemical Engineering and Chemistry, Eindhoven University of Technology, 5612 AZ Eindhoven, The Netherlands; Institute for Complex Molecular Systems, Eindhoven University of Technology, 5612 AZ Eindhoven, The Netherlands;* orcid.org/0000-0002-3485-1984; Email: a.p.h.j.schenning@tue.nl

Cees W. M. Bastiaansen − *Laboratory of Stimuli-responsive Functional Materials & Devices (SFD), Department of Chemical Engineering and Chemistry, Eindhoven University of Technology, 5612 AZ Eindhoven, The Netherlands; School of Engineering and Materials Science, Queen Mary, University of London, London E1 4NS, United Kingdom;* orcid.org/0000-0003-1198-7528; Email: c.w.m.bastiaansen@tue.nl

Authors

Xinglong Pan − *Laboratory of Stimuli-responsive Functional Materials & Devices (SFD), Department of Chemical Engineering and Chemistry, Eindhoven University of Technology, 5612 AZ Eindhoven, The Netherlands*

Michael G. Debije − *Laboratory of Stimuli-responsive Functional Materials & Devices (SFD), Department of Chemical Engineering and Chemistry, Eindhoven University of Technology, 5612 AZ Eindhoven, The Netherlands;* orcid.org/0000-0001-8844-1115

Complete contact information is available at: https://pubs.acs.org/10.1021/acsami.1c06415

Notes

The authors declare no competing financial interest.

ACKNOWLEDGMENTS

We acknowledge Ir. Sean J. D. Lugger, Ir. Simon J. A. Houben, and Ing. Tom A. B. P. Bus for practical support. This work was funded by the China Scholarship Council.

REFERENCES

(1) Verpaalen, R. C. P.; Engels, T.; Schenning, A. P. H. J.; Debije, M. G. Stimuli-Responsive Shape Changing Commodity Polymer Composites and Bilayers. *ACS Appl. Mater. Interfaces* **2020**, *12*, 38829.

(2) Xu, X.; Zhou, J.; Chen, J. Thermal Transport in Conductive Polymer-Based Materials. *Adv. Funct. Mater.* **2020**, *30*, 1904704.

(3) Huang, C.; Qian, X.; Yang, R. Thermal Conductivity of Polymers and Polymer Nanocomposites. *Mater Sci Eng R: Rep.* **2018**, *132*, 1−22.

(4) Han, Z.; Fina, A. Thermal Conductivity of Carbon Nanotubes and Their Polymer Nanocomposites: A Review. *Prog. Polym. Sci.* **2011**, *36*, 914−944.

(5) Chen, H.; Ginzburg, V. V.; Yang, J.; Yang, Y.; Liu, W.; Huang, Y.; Du, L.; Chen, B. Thermal Conductivity of Polymer-Based Composites: Fundamentals and Applications. *Prog. Polym. Sci.* **2016**, *59*, 41−85.

(6) Zhang, Y.; Heo, Y. J.; Son, Y. R.; In, I.; An, K. H.; Kim, B. J.; Park, S. J. Recent Advanced Thermal Interfacial Materials: A Review of Conducting Mechanisms and Parameters of Carbon Materials. *Carbon* **2019**, *142*, 445−460.

(7) Xu, X.; Chen, J.; Zhou, J.; Li, B. Thermal Conductivity of Polymers and Their Nanocomposites. *Adv. Mater.* **2018**, *30*, 1705544.

(8) Saeidijavash, M.; Garg, J.; Grady, B. P.; Smith, B.; Li, Z.; Young, R. J.; Tarranum, F.; Bel Bekri, N. High Thermal Conductivity through Simultaneously Aligned Polyethylene Lamellae and Graphene Nanoplatelets. *Nanoscale* **2017**, *9*, 12867−12873.

(9) Pan, X.; Shen, L.; Schenning, A. P. H. J.; Bastiaansen, C. W. M. Transparent, High-Thermal-Conductivity Ultradrawn Polyethylene/Graphene Nanocomposite Films. *Adv. Mater.* **2019**, *31*, 1904348.

(10) Pan, X.; Schenning, A. H. P. J.; Shen, L.; Bastiaansen, C. W. M. The Role of Polyethylene Wax on the Thermal Conductivity of Transparent Ultradrawn Polyethylene Films. *Macromolecules* **2020**, *53*, 5599.

(11) Xu, Y.; Kraemer, D.; Song, B.; Jiang, Z.; Zhou, J.; Loomis, J.; Wang, J.; Li, M.; Ghasemi, H.; Huang, X.; Li, X.; Chen, G. Nanostructured Polymer Films with Metal-like Thermal Conductivity. *Nat. Commun.* **2019**, *10*, 1771.

(12) Shen, S.; Henry, A.; Tong, J.; Zheng, R.; Chen, G. Polyethylene Nanofibres with Very High Thermal Conductivities. *Nat. Nanotechnol.* **2010**, *5*, 251−255.

(13) Shrestha, R.; Li, P.; Chatterjee, B.; Zheng, T.; Wu, X.; Liu, Z.; Luo, T.; Choi, S.; Hippalgaonkar, K.; De Boer, M. P.; Shen, S. Crystalline Polymer Nanofibers with Ultra-High Strength and Thermal Conductivity. *Nat. Commun.* **2018**, *9*, 1664.

(14) Shrestha, R.; Luan, Y.; Shin, S.; Zhang, T.; Luo, X.; Lundh, J. S.; Gong, W.; Bockstaller, M. R.; Choi, S.; Luo, T.; Chen, R.; Hippalgaonkar, K.; Shen, S. High-Contrast and Reversible Polymer Thermal Regulator by Structural Phase Transition. *Sci. Adv.* **2019**, *5*, 3777.

(15) Park, Y.; You, M.; Shin, J.; Ha, S.; Kim, D.; Heo, M. H.; Nah, J.; Kim, Y. A.; Seol, J. H. Thermal Conductivity Enhancement in Electrospun Poly(Vinyl Alcohol) and Poly(Vinyl Alcohol)/Cellulose Nanocrystal Composite Nanofibers. *Sci. Rep.* **2019**, *9*, 3026.
(16) Zhuang, Y.; Zheng, K.; Cao, X.; Fan, Q.; Ye, G.; Lu, J.; Zhang, J.; Ma, Y. Flexible Graphene Nanocomposites with Simultaneous Highly Anisotropic Thermal and Electrical Conductivities Prepared by Engineered Graphene with Flat Morphology. *ACS Nano* **2020**, *14*, 11733.
(17) Chen, A.; Wu, Y.; Zhou, S.; Xu, W.; Jiang, W.; Lv, Y.; Guo, W.; Chi, K.; Sun, Q.; Fu, T.; Xie, T.; Zhu, Y.; Liang, X. G. High Thermal Conductivity Polymer Chains with Reactive Groups: A Step towards True Application. *Mater Adv* **2020**, *1*, 1996.
(18) Chien, H. C.; Peng, W. T.; Chiu, T. H.; Wu, P. H.; Liu, Y. J.; Tu, C. W.; Wang, C. L.; Lu, M. C. Heat Transfer of Semicrystalline Nylon Nanofibers. *ACS Nano* **2020**, *14*, 2939−2946.
(19) Xu, Y.; Wang, X.; Zhou, J.; Song, B.; Jiang, Z.; Lee, E. M. Y.; Huberman, S.; Gleason, K. K.; Chen, G. Molecular Engineered Conjugated Polymer with High Thermal Conductivity. *Sci. Adv.* **2018**, *4*, 3031.
(20) Hummel, P.; Lechner, A. M.; Herrmann, K.; Biehl, P.; Rössel, C.; Wiedenhöft, L.; Schacher, F. H.; Retsch, M. Thermal Transport in Ampholytic Polymers: The Role of Hydrogen Bonding and Water Uptake. *Macromolecules* **2020**, *53*, 5528.
(21) Pan, X.; Debije, M. G.; Schenning, A. P. H. J. High Thermal Conductivity in Anisotropic Aligned Polymeric Materials. *ACS Appl Polym Mater* **2021**, *3*, 578.
(22) Yamaura, K.; Tanigami, T.; Hayashi, N.; Kosuda, K. I.; Okuda, S.; Takemura, Y.; Itok, M.; Matsuzawa, S. Preparation of High Modulus Poly(Vinyl Alcohol) by Drawing. *J. Appl. Polym. Sci.* **1990**, *40*, 905−916.
(23) Xie, X.; Li, D.; Tsai, T.-H.; Liu, J.; Braun, P. V.; Cahill, D. G. Thermal Conductivity, Heat Capacity, and Elastic Constants of Water-Soluble Polymers and Polymer Blends. *Macromolecules* **2016**, *49*, 972−978.
(24) Yano, T.; Higaki, Y.; Tao, D.; Murakami, D.; Kobayashi, M.; Ohta, N.; Koike, J. I.; Horigome, M.; Masunaga, H.; Ogawa, H.; Ikemoto, Y.; Moriwaki, T.; Takahara, A. Orientation of Poly(Vinyl Alcohol) Nanofiber and Crystallites in Non-Woven Electrospun Nanofiber Mats under Uniaxial Stretching. *Polymer* **2012**, *53*, 4702.
(25) Kongkhlang, T.; Tashiro, K.; Kotaki, M.; Chirachanchai, S. Electrospinning as a New Technique to Control the Crystal Morphology and Molecular Orientation of Polyoxymethylene Nanofibers. *J. Am. Chem. Soc.* **2008**, *130*, 15460.
(26) Tarani, E.; Terzopoulou, Z.; Bikiaris, D. N.; Kyratsi, T.; Chrissafis, K.; Vourlias, G. Thermal Conductivity and Degradation Behavior of HDPE/Graphene Nanocomposites: Pyrolysis, Kinetics and Mechanism. *J. Therm. Anal. Calorim.* **2017**, *129*, 1715−1726.
(27) Gu, J.; Li, N.; Tian, L.; Lv, Z.; Zhang, Q. High Thermal Conductivity Graphite Nanoplatelet/UHMWPE Nanocomposites. *RSC Adv.* **2015**, *5*, 36334−36339.
(28) Che, J.; Wu, K.; Lin, Y.; Wang, K.; Fu, Q. Largely Improved Thermal Conductivity of HDPE/Expanded Graphite/Carbon Nanotubes Ternary Composites via Filler Network-Network Synergy. *Compos Part A Appl Sci Manuf* **2017**, *99*, 32−40.
(29) Zhang, W. B.; Zhang, Z. X.; Yang, J. H.; Huang, T.; Zhang, N.; Zheng, X. T.; Wang, Y.; Zhou, Z. W. Largely Enhanced Thermal Conductivity of Poly(Vinylidene Fluoride)/Carbon Nanotube Composites Achieved by Adding Graphene Oxide. *Carbon* **2015**, *90*, 242−254.
(30) Ronca, S.; Igarashi, T.; Forte, G.; Rastogi, S. Metallic-like Thermal Conductivity in a Lightweight Insulator: Solid-State Processed Ultra High Molecular Weight Polyethylene Tapes and Films. *Polymer* **2017**, *123*, 203−210.
(31) Song, S.; Zhang, Y. Carbon Nanotube/Reduced Graphene Oxide Hybrid for Simultaneously Enhancing the Thermal Conductivity and Mechanical Properties of Styrene-Butadiene Rubber. *Carbon* **2017**, *123*, 158−167.
(32) Shtein, M.; Nadiv, R.; Buzaglo, M.; Regev, O. Graphene-Based Hybrid Composites for Efficient Thermal Management of Electronic Devices. *ACS Appl. Mater. Interfaces* **2015**, *7*, 23725−23730.
(33) Alam, F. E.; Dai, W.; Yang, M.; Du, S.; Li, X.; Yu, J.; Jiang, N.; Lin, C. T. In Situ Formation of a Cellular Graphene Framework in Thermoplastic Composites Leading to Superior Thermal Conductivity. *J. Mater. Chem. A* **2017**, *5*, 6164−6169.
(34) Kashyap, S.; Pratihar, S. K.; Behera, S. K. Strong and Ductile Graphene Oxide Reinforced PVA Nanocomposites. *J. Alloys Compd.* **2016**, *684*, 254−260.
(35) Li, J.; Shao, L.; Zhou, X.; Wang, Y. Fabrication of High Strength PVA/RGO Composite Fibers by Gel Spinning. *RSC Adv.* **2014**, *4*, 43612−43618.
(36) Dai, L.; Ying, L. Infrared Spectroscopic Investigation of Hydrogen Bonding in EVOH Containing PVA Fibers. *Macromol. Mater. Eng.* **2002**, *287*, 509−514.
(37) Tan, L.; Wan, A. Structural Changes in Thermal-Induced Polyacrylonitrile Gel under Uniaxial Drawing. *Colloids Surf. A Physicochem Eng Asp* **2011**, *392*, 350−354.

https://doi.org/10.1021/acsami.1c06415
ACS Appl. Mater. Interfaces 2021, 13, 28864−28869